TMPM Tschermaks Min. Petr. Mitt. 29, 223–240 (1982)

TMPM Tschermaks Mineralogische und Petrographische Mitteilungen

From the Istituto di Mineralogia, Cristallografia e Geochimica, Università di Torino, Italy, and the Istituto di Mineralogia e Petrologia, Università di Padova, Italy

Crystal Structures of Ca-rich Clinopyroxenes on the $CaMgSi_2O_6-Mg_2Si_2O_6$ Join

E. Bruno, Susanna Carbonin, and **G. Molin**

With 6 Figures

Received August 10, 1981;
accepted September 28, 1981

Summary

The structural changes occurring in the clinopyroxenes with composition Di100, Di90En10 and Di80En20, due to the Ca-Mg substitution in the M2 site, have been studied. Evidence is given that with increasing Mg content a small percentage of the atoms converts from the M2 position to a new M2′ position which is solely occupied by Mg. The maximum conversion of M2 to M2′ found in this study is 7%. The closest parallel to the M2′ geometry is found in the $ZnSiO_3$ pyroxene ($C2/c$). The presence of this new site causes significant changes in the tetrahedral configuration, because the M2′ atoms are not bonded to O3. The intermediate compositions, Di90En10 and Di80En20, may be thought of as the coexistence of two structural models: diopside and $ZnSiO_3$ pyroxene ($C2/c$).

Zusammenfassung

Kristallstrukturen Ca-reicher Klinopyroxene der $CaMgSi_2O_6 - Mg_2Si_2O_6$-Reihe

Es wurden die strukturellen Änderungen von Klinopyroxenen der Zusammensetzungen Di100, Di90En10 und Di80En20, die durch den Mg-Ersatz für Ca verursacht werden, untersucht. Es zeigt sich, daß mit steigendem Mg-Gehalt ein kleiner Teil der Atome der M2-Position zu einer neuen M2′-Position wechselt; diese wird ausschließlich durch Mg besetzt. Der größte in dieser Arbeit gefundene Übergang von M2 nach M2′ beträgt ca. 7%. Die stärksten Parallelen zur Geometrie um M2′ werden im Pyroxen $ZnSiO_3$ ($C2/c$) gefunden. Die Besetzung dieser neuen Position verursacht bedeutende Änderungen im Tetraederverband, da die M2′-Atome nicht an O3 gebunden sind.
Die Pyroxenstrukturen mit den intermediären Zusammensetzungen Di90En10 und Di80En20 können als Überlagerung zweier Modelle betrachtet werden: Diopsid und $ZnSiO_3$-Pyroxen ($C2/c$).

Abbreviations

En = Enstatite, Di = Diopside, Hd = Hedenbergite, Fs = Ferrosilite, ClEn = Clinoenstatite, Di100 = pure diopside, Di90 = Di90En10 (mol.-%), Di80 = Di80En20, brg. = bridging.

0041-3763/82/0029/0223/$ 03.60

Introduction

During a crystal chemical study of a series of natural $C2/c$ pyroxenes (*Dal Negro* et al., 1982) undertaken to deduce the site occupancies in the multi site solid solutions, it was realized that the site occupancy data on the binary join Di-En were not available. These solutions are important because of the substitution in the M2 site of cations of quite different size, Ca and Mg, resulting in very different geometrical features, which are not well explained in natural compounds.
The Di-En join is a useful geothermometer and its phase relationships have been extensively studied (*Atlas*, 1952; *Boyd* and *Schairer*, 1964; *Davis* and *Boyd*, 1966; *Kushiro*, 1972; *Warner* and *Luth*, 1974; *Nehru* and *Wyllie*, 1974; *Mori* and *Green*, 1975 and 1976; *Howells* and *O'Hara*, 1975; *Lindsley* and *Dixon*, 1976; *Newton* et al., 1979). There is a close dependence of the solvus on temperature but pressure particularly at low temperatures has a minor influence.
From a structural point of view in the Mg-rich region, three polymorphs of $MgSiO_3$: orthoenstatite (*Morimoto* and *Koto*, 1969), protoenstatite (*Smith*, 1959) low clinoenstatite (*Morimoto* et al., 1960) have been identified. *Ohashi* and *Finger* (1976) have studied two compositions with a small amount of Ca in solid solution (ClEn89Di11 and ClEn83Di17). In addition *Smith* (1969) proposed a $C2/c$ high clinoenstatite polymorph, probably favored by substitution of Ca for Mg. *Schwab* and *Schwerin* (1975) confirmed this hypothesis observing the transition low ClEn – high $C2/c$ at 1050°C for En90Di10 composition.
In the Ca-rich region the only one phase observed is $C2/c$. The structural data are scarce except for diopside (*Clark* et al., 1969; *Levien* and *Prewitt*, 1981). Our work is concerned with the study of the structural changes occurring in the solid solutions between diopside and enstatite on the Ca-rich side of the join.

Synthesis and Chemical Analyses of Pyroxenes

The compositions of crystals studied were Di100, Di90En10 and Di80En20 (in molecular proportions of diopside and enstatite in solid solutions), hereafter referred to as Di100, Di90, Di80 respectively[1].

---

[1] A microprobe investigation with an X-Ray energy dispersive system was carried out on several fragments of these synthetic crystals using augite from Kakanui, New Zealand, as standard. No appreciable inhomogeneity was detected except for some areas (of about 5 μ diameter) of pure SiO_2. The resulting compositions were: $Ca_{1.00}Mg_{1.01}Si_{1.99}O_6$ for Di100; $Ca_{0.89}Mg_{1.11}Si_{1.98}O_6$ for Di90 and $Ca_{0.80}Mg_{1.20}Si_{1.99}O_6$ for Di80.

The starting materials were gels prepared from $CaCO_3$ (99% purity, Merck, dried for 4 hrs at 400°C), Mg metal (99.8%, C. Erba), and Teos (tetraetil-orthosilicate, Merck) as suggested by *Biggar* and *O'Hara* (1969). These gels were fused to glasses at 1420°C in an electric furnace and quickly quenched in air. The glasses were crystallized at the following conditions: Di100 at 1370°C for 130 hrs; Di90 and Di80 at 1330°C for 130 hrs.

Table 1. *Unit Cell Parameters* (Å, estimated standard errors refer to the last digit), unit cell volumes (Å^3) and collection data

Samples	a	b	c	β	V	no. meas. refl.	no. obs. refl. $I>2\sigma(I)$	R%
Di100	9.750 (1)	8.926 (1)	5.251 (1)	105.90 (1)	439.50	649	542	2.0
Di90	9.738 (1)	8.918 (1)	5.248 (1)	106.08 (1)	437.92	653	526	2.1
Di80	9.734 (1)	8.917 (1)	5.247 (1)	106.33 (1)	437.06	650	527	2.6

Experimental Data

The samples were examined with a petrographic microscope for fragments optically homogeneous and with sharp extinction. Three crystals were chosen for the X-Ray data collection using the same procedure for all the samples. The equipment used was a single-crystal automatic diffractometer Philips PW1100 with MoK_α radiation monochromatized by a flat graphite crystal. The intensities of the reflections with $\theta \leqslant 30°$ were collected using the ω scan mode; the equivalent hkl and $h\bar{k}l$ pairs were scanned. The intensities were corrected for absorption following the semi-empirical method of *North* et al. (1968) and the values of the equivalent pairs averaged.
The X-Ray data were processed with a program specifically written for the PW1100 diffractometer (*Hornstra* and *Stubbe*, 1972). The unit cell parameters (Table 1) were obtained with one of the standard programs of the Philips PW1100 diffractometer (LAT program).

X-Ray Structure Refinements

All refinements were carried out in the space group $C2/c$ starting with the atomic coordinates of diopside (*Clark* et al., 1969). A locally re-written version of the full-matrix least-squares program ORFLS (*Busing* et al., 1962) was used.
Particular attention was paid in the choice of the scattering factors to be assigned to the sites: while fully ionized cations were considered in the M2 and M1 sites, both neutral and totally ionized atoms (with 0.625 percentage

of Si^{4+}) were used for the tetrahedral site (*International Tables for X-Ray Crystallography*, 1974). A 0.50 occupancy of O^{1-} against $O^{2-}$was used for the oxygen atoms (*Tokonami*, 1965). Since the maximum difference between the neutral and ionized scattering curves occurs at low (up to 0.30) $\sin\theta/\lambda$ values, this choice was necessary to obtain the best $F_o - F_c$ agreement. The occupancies at the M2 and M1 sites were processed on the basis of ORFLS program (*Busing* et al., 1962). In Di90 and Di80 the scattering factors of Ca^{2+} vs. Mg^{2+} were assigned to M2 with the constraint $Ca^{2+} + Mg^{2+} = 1$. The scattering factor of Mg^{2+} was assigned to M1 site. Di100 has been refined with a fixed full occupancy of Ca^{2+} in M2 and Mg^{2+} in M1 sites (no substantial differences have been observed in the occupancies after a trial refinement in which both M2 and M1 occupancies were allowed to vary).
The reflections with $I > 2\sigma(I)$ were utilized for the refinements using unit weights (Table 1).
In the first stages of these refinements isotropic temperature factors were used and successively all the atoms were treated anisotropically. Scale factors, secondary extinction coefficients (*Zachariasen*, 1963), atomic coordinates, thermal parameters, site occupancies, were allowed to vary together in each least-squares cycle (Table 2). When the anisotropic refinements reached convergence, difference Fourier syntheses were computed and residual electron density was observed in Di90 and Di80 approximately positioned at 0.7 Å from the M2 site along the y axis (see *Rossi* et al., 1978; *Dal Negro* et al., 1982).
In the final cycles of refinements this residual, called M2′, was introduced with a temperature factor equal to the isotropic T factor of the M2 site. The scattering curve of Mg^{2+} was assigned to it and only the occupancy factor was allowed to vary alternately with scale factor, secondary extinction coefficient, atomic coordinates, thermal parameters, M2 site occupancy, varying all together (Table 2). The R discrepancy factors after these cycles dropped significantly from 2.4 to 2.1 in Di90 and from 3.1 to 2.6 in Di80[2].

The Site M2′

The electron residual observed by the difference Fourier syntheses in Di90 and Di80 as noted before, is situated between the y parameters of M2 and M1 nearly 0.22 of fractional coordinate value (Table 2). The interatomic distances of this site from O1 and O2 oxygen atoms are 1.84 Å and 2.29 Å for Di90 and 1.84 and 2.26 Å for Di80, but the distances with the O3 atoms exceed 3 Å (see Table 3). Accordingly M2′ is four-coordinated with a mean interatomic distance of 2.065 Å for Di90 and 2.050 Å for Di80. This is similar

[2] Observed and calculated structure factors available from S. Carbonin.

Table 2. *Fractional Atomic Coordinates, Equivalent Isotropic Temperature Factors (after Hamilton, 1959) and Site Occupancies Where Refined (estimated standard errors refer to the last digit).* The occupancies are expressed in number of electron units of the fully ionized cations considered in the sites (e.g.: M2 occupancy Di90 = 16.9 e^- = (0.87×18)e^- + (0.13×10) e^- where 0.87 and 0.13 are site occupancies, see text)

		Di100	Di90	Di80
M2	*y/b*	0.3011 (1)	0.3000 (1)	0.2983 (1)
	B (Å^2)	0.54	0.59	0.64
	occ. (e^-)	18	16.9 (1)	15.7 (1)
M1	*y/b*	0.9082 (1)	0.9079 (1)	0.9075 (1)
	B (Å^2)	0.32	0.38	0.40
	occ. (e^-)	10	9.9 (1)	9.9 (1)
O3	*x/a*	0.3507 (1)	0.3507 (1)	0.3506 (2)
	y/b	0.0179 (1)	0.0186 (1)	0.0195 (2)
	z/c	− 0.0043 (3)	− 0.0037 (2)	− 0.0018 (3)
	B (Å^2)	0.55	0.52	0.61
O2	*x/a*	0.3615 (1)	0.3623 (1)	0.3635 (2)
	y/b	0.2496 (2)	0.2492 (1)	0.2492 (2)
	z/c	0.3196 (3)	0.3225 (3)	0.3264 (3)
	B (Å^2)	0.61	0.68	0.85
O1	*x/a*	0.1159 (1)	0.1162 (1)	0.1166 (2)
	y/b	0.0877 (1)	0.0877 (1)	0.0882 (2)
	z/c	0.1423 (2)	0.1432 (2)	0.1434 (3)
	B (Å^2)	0.44	0.42	0.44
T	*x/a*	0.2866 (1)	0.2872 (1)	0.2881 (1)
	y/b	0.0933 (1)	0.0932 (1)	0.0929 (1)
	z/c	0.2302 (1)	0.2318 (1)	0.2340 (1)
	B (Å^2)	0.31	0.32	0.32
M2′	*y/b*		0.2227	0.2217
	occ. (e^-)		0.4	0.7

to the coordination of Zn(2) in the $ZnSiO_3$ *C2/c* pyroxene synthetized by *Morimoto* et al. (1975).

This pyroxene has M1 and M2 fully occupied by Zn, but with different coordinations. While M1 is octahedrally coordinated, the M2 site shows "an irregular tetrahedral coordination of the O1 and O2 atoms around Zn(2)" and has atomic coordinates $x = 0.0, y = 0.2361(1), z = 0.25$.

The analogies between the coordinates of M2′ and Zn(2) and between the shapes of their polyhedra are particularly close and make us conclude that this new site M2′ is very similar to the M2 of $ZnSiO_3$ monoclinic synthetic pyroxene.

Takeda (1972) described an unstable four-coordinated M2 situation in Ca-rich pyroxenes near the miscibility gap but took into account only mean values of M2 configuration. However *Rossi* et al. (1978) considered the possibility that there may be a distinct M2′ site as found by us.

Table 3. *Polyhedral Geometry in M2 and M2′ Sites*

	Di100	Di90	Di80
M2–O2C2, D2[a]	2.337 (1)	2.314 (2)	2.285 (2)
M2–O1A1, B1	2.361 (1)	2.351 (2)	2.335 (2)
M2–O3C1, D1	2.566 (1)	2.573 (2)	2.585 (2)
M2–O3C2, D2	2.724 (1)	2.729 (2)	2.744 (2)
mean of 8	2.497	2.492	2.487
V (Å^3)	25.73	25.53	25.37
ΔM2[b]	0.303	0.316	0.342
M2′–O2C2, D2		2.29	2.26
M2′–O1A1, B1		1.84	1.84
mean of 4		2.065	2.050
O2C1–M2′–O2D1		167.4 (1)	166.8 (1)
O2C1–M2′–O1A1		97.3 (1)	97.5 (1)
O2C1–M2′–O1B1		90.9 (1)	91.0 (1)
O1A1–M2′–O1B1		98.4 (1)	99.2 (1)
M1–M2′		2.81	2.80

[a] Atom nomenclature is after *Burnham* et al. (1967).

[b] $\Delta M2 = M2\text{–}O3C2 - \overline{(M2\text{–}O3C1 + M2\text{–}O2 + M2\text{–}O1)}$, see text.

The occupancies of M2′ after the final cycles of the refinements were estimated to 0.4e$^-$ and 0.7 e$^-$ in Di90 and Di80 respectively, corresponding to an occupancy of 0.04 and 0.07 of Mg atomic fraction (see Table 2). It is therefore a clear indication that there is an increase in this value with the increase of the En content. However this correlation needs confirmation from further work because at present the double electron displacement related to the M2 site (M2 and M2′) causes anomalous situation in the treatment of the occupancy determination.

Moreover taking into consideration the mean M2′–O distances from O1 and O2 atoms (2.065 Å for Di90 and 2.050 Å for Di80), which are not different from an average Mg–O bond length, we can reasonably suggest that M2′ is occupied by Mg.

The Site M2

In spite of the small range of solid solution from Di100 to Di80 the radius difference between Ca and Mg causes a very significant rearrangement in the M2 polyhedron. As it can be seen in Table 3 the smaller bond lengths M2–O2 and M2–O1 decrease significantly with the increase of Mg in solid solution, while M2–O3C1 and M2–O3C2 increase.

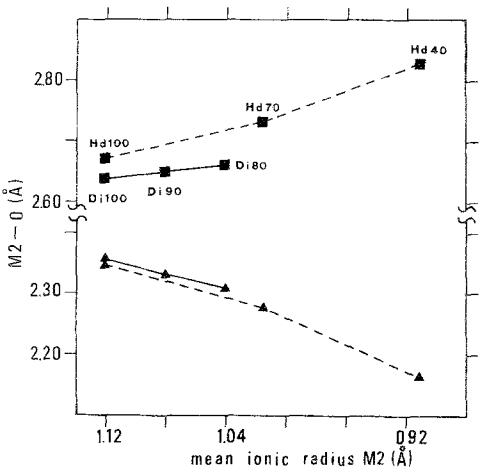

Fig. 1. $\overline{M2-O}$ brg. (squares) and $\overline{M2-O}$ non brg. (triangles) interatomic distances *vs.* mean atomic radius in M2 in Ca–Mg (continuous line) and Ca–Fe (dotted line) series. Atomic radii according to *Shannon* and *Prewitt* (1969)

The M2–O2 interatomic distances, ranging from 2.337 Å in Di100 to 2.285 Å in Di80, seem to be the most sensitive to the Mg–Ca replacement.
A parameter indicative of the distortion of the M2 polyhedron was calculated and called ΔM2. It is equal to the difference between the longest M2–O3C2 bond length and the average of the three shortest ones which constitute by themselves the symmetric half of a hypothetical octahedron M2–O3C2–$\overline{(M2-O3C1 + M2-O2 + M2-O1)}$. ΔM2 can be useful because it is good correlated both with the electrons in the M2 polyhedron (Table 2) and with β crystallographic parameter (Table 1).
As regard the rearrangement of the M2 site from Di100 to Di80 note that:
1) the change in the y fractional coordinate of the unit cell parameter (from 0.3011(1) to 0.2983(1)) is rather low;
2) the thermal vibration ellipsoids (Table 6) do not show abnormally large anisotropy with the increase of En content.

These two considerations, compared with the effects caused by the Ca–Fe substitution in the Hd–Fs join (*Cameron* et al., 1973; *Ohashi* et al., 1975), show that the mechanisms of the Ca–Mg and Ca–Fe substitutions are not strictly the same. The displacement of M2 in the Hd–Fs series in fact is much more pronounced as it can be seen from the y fractional coordinates of M2 (Hd100 y = 0.3003(1); Hd70 y = 0.2908(1); Hd40 y = 0.2751(1)).
In addition the r.m.s. amplitudes along the b-axis change from 0.084(1) (Hd100) to 0.209(2) (Hd40) showing a rather high anisotropy (*Cameron* et al., 1973; *Ohashi* et al., 1975).
Fig. 1 shows the M2–O bond lengths plotted against the mean M2 atomic radius in the Hd–Fs and Di–En series. The M2–O bond length in the Fe-bearing pyroxenes changes more significantly with the mean atomic radius than in the Mg-bearing pyroxenes. The M2–O distances are particularly susceptible to the M2 atomic displacement. Therefore there is only little positional disorder in the Di–En series with increasing substitution of Ca by Mg.

The Site M1

Chemically the M1 site is simple because of its occupancy by Mg only (Table 2). Therefore the variations shown by the structural data (Table 4) can only be ascribed to the changes occurring in the M2 polyhedron.
The geometry of the M1 site has been represented by the $\lambda^{\S}_{oct} - \sigma^{2\blacktriangle}_{oct}$ (*Robinson* et al., 1971) and by the $\Delta^{\blacksquare}_{oct} - \sigma^2_{oct}$ (*Fleet*, 1976) diagrams (Fig. 2) which represent in a similar way the elongation of this polyhedron along our series. Both diagrams are characterized by two trends: the first shows only one variable, the σ^2, which decreases from Di100 to Di90; the second, from Di90 to Di80, is characterized above all by the increase of λ_{oct} (Δ_{oct}) as shown by the significant change of the M1–O1A1, B1 distances from 2.125 Å to 2.136 Å (Table 4).

---

§ $\langle \lambda_{oct} \rangle = \sum_{i=1}^{6} (l_i/l_0)^2/6$ = "mean octahedral quadratic elongation parameter, where l_0 is the center-to-vertex distance of an octahedron with O_h symmetry whose volume is equal to that of the strained or distorted octahedron with bond lengths l_i".

▲ $\sigma^2_{\theta\,oct} = \sum_{i=1}^{12} (\theta_i - 90°)^2/11$ = "variance of the octahedral angles".

■ $\Delta_{oct} = 1/6 \sum_{i=1}^{6} [(l_i - \bar{l})/\bar{l}]^2$ = "mean square relative deviation from average bond length, where $\bar{l}$ is the mean bond length (*Brown* and *Shannon*, 1973)".

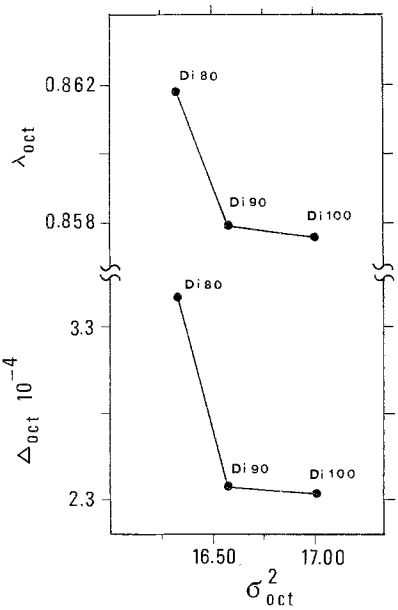

Fig. 2. σ^2_{oct} *vs.* Δ_{oct} or λ_{oct} diagrams (see Table 4)

Table 4. *Bond Lengths and Angles in M1 Site*

	Di100	Di90	Di80
M1–O2C1, D1	2.057 (1)	2.056 (2)	2.054 (2)
M1–O1A2, B2	2.060 (1)	2.060 (1)	2.056 (2)
M1–O1A1, B1	2.125 (1)	2.125 (2)	2.136 (2)
mean of 6	2.081	2.080	2.082
V (Å^3)	11.92	11.92	11.94
O2D1–M1–O2C1	93.0 (1)	93.0 (1)	93.2 (1)
O2D1–M1–O1B1	92.8 (1)	92.8 (1)	92.7 (1)
O2D1–M1–O1B2	89.0 (1)	89.6 (1)	90.2 (1)
O2D1–M1–O1A2	92.4 (1)	91.9 (1)	91.2 (1)
O1A1–M1–O1B1	82.1 (1)	82.0 (1)	81.9 (1)
O1A1–M1–O1B2	84.6 (1)	84.6 (1)	84.6 (1)
O1A1–M1–O1A2	93.8 (1)	93.7 (1)	93.7 (1)
λ_{oct} [a]	0.8576	0.8579	0.8618
Δ_{oct} [b]	2.33×10^{-4}	2.36×10^{-4}	3.47×10^{-4}
σ^2_{oct} [c]	17.00	16.57	16.33

[a] λ_{oct} (*Robinson* et al., 1971) defined by $\sum_{i=1}^{6}(l_i/l_0)^2/6$.

[b] Δ_{oct} (*Fleet*, 1976) defined by $1/6\sum_{i=1}^{6}[(l_i-\bar{l})/\bar{l}]^2$.

[c] $\sigma^2_{\theta\,oct}$ (*Robinson* et al., 1971) defined by $\sum_{i=1}^{12}(\theta_i-90°)^2/11$.

Considering that both M1 and M2′ share the O1A1, O1B1 atoms, the lengthening of the M1–O1A1, B1 distances from Di90 to Di80 may be attributed to a higher concentration of Mg in M2′.

The Tetrahedron

The principal rearrangement in the T–O–T chain are primarily caused by the presence of M2′ site which, by losing the O3 atoms and by linking the O2 and O1 oxygens, causes charge imbalance in the tetrahedron and other changes in it throughout.

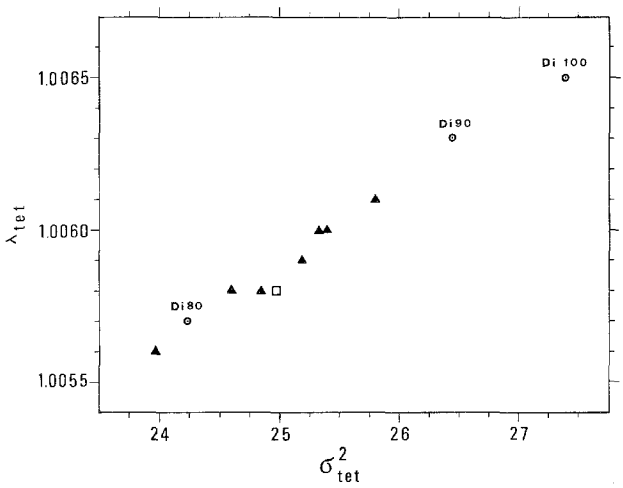

Fig. 3. σ^2_{tet} *vs.* λ_{tet} diagram (see Table 5). Augite samples (triangles) (*Dal Negro* et al., 1982), Hedenbergite (square) (*Cameron* et al., 1973) σ^2_{tet} (Hd) from *Cameron* et al. (1973), λ_{tet} (Hd) calculated by present authors from the data of *Cameron* et al. (1973) in according to the formula of *Robinson* et al. (1971)

The geometry of the T site is shown by the $\lambda^{\blacktriangle}_{tet} - \sigma^{2\,\blacksquare}_{tet}$ diagram (*Robinson* et al., 1971) which shows a maximum distortion for the M2-Mg-poor members (Table 5 and Fig. 3). The T distortion of diopside is more conspicuous than such distortions in natural augites studied by us (*Dal Negro* et al., 1982).

▲ $<\lambda_{tet}> = \sum_{i=1}^{4} (l_i/l_0)^2/4$ = "mean tetrahedral quadratic elongation parameter, where l_0 is the center-to-vertex distance for a tetrahedron whose volume is equal to that of the strained or distorted tetrahedron with bond lengths l_i".

■ $\sigma^2_{\theta\,tet} = \sum_{i=1}^{6} (\theta_i - 109.47°)^2/5$ = "variance of the tetrahedral angles".

Table 5. *Polyhedral Geometry in the T Site*

	Di100	Di90	Di80
T–O2	1.585 (1)	1.583 (2)	1.585 (2)
T–O1	1.601 (1)	1.601 (1)	1.603 (2)
mean, non brg.	1.593	1.592	1.594
T–O3A1	1.667 (1)	1.665 (2)	1.658 (2)
T–O3A2	1.686 (1)	1.682 (1)	1.681 (2)
mean, brg.	1.676	1.673	1.669
mean of 4	1.635	1.633	1.632
T–TA2	3.109 (1)	3.106 (1)	3.103 (1)
V (Å^3)	2.223	2.215	2.213
O3A1–O3A2	2.645 (1)	2.645 (1)	2.647 (1)
O2–O3A1	2.661 (2)	2.658 (2)	2.655 (3)
O2–O3A2	2.574 (2)	2.571 (2)	2.575 (3)
O1–O3A2	2.691 (2)	2.684 (2)	2.683 (3)
O1–O2	2.733 (2)	2.731 (2)	2.731 (3)
O1–O3A1	2.680 (2)	2.677 (2)	2.668 (3)
O3A1–T–O3A2	104.1 (1)	104.4 (1)	104.8 (1)
O3A1–T–O2	109.8 (1)	109.8 (1)	109.9 (1)
O3A1–T–O1	110.1 (1)	110.0 (1)	109.8 (1)
O3A2–T–O2	103.7 (1)	103.8 (1)	104.1 (1)
O3A2–T–O1	109.9 (1)	109.7 (1)	109.6 (1)
O2–T–O1	118.1 (1)	118.1 (1)	117.9 (1)
T–O3–TA2	136.0 (1)	136.2 (1)	136.7 (1)
O3A2–O3A1–O3A2	166.1 (1)	165.6 (1)	164.9 (2)
λ_{tet} [a]	1.0065	1.0063	1.0057
σ^2_{tet} [b]	27.39	26.45	24.23
tilting angles [c]	2.6	2.8	3.1

[a] λ_{tet} (*Robinson* et al., 1971) defined by $\sum_{i=1}^{4} (l_i/l_0)^2/4$.

[b] $\sigma^2_{\theta tet}$ (*Robinson* et al., 1971) defined by $\sum_{i=1}^{6} (\theta_i - 109.47°)^2/5$.

[c] Tilting angles between (100) crystallographic plane and the basal face O2–O3–O3 of a tetrahedron.

In Fig. 3 we have also plotted the $\lambda_{tet} - \sigma^2_{tet}$ values for Hd (*Cameron* et al., 1973) which fall in intermediate position. Note that with M2 fully occupied by Ca, the smaller is the radius of the ion in M1, the greater is the distortion of the tetrahedron (see also *Cameron* and *Papike*, 1981).

Table 5 shows that while the $\overline{T-O}$ brg. and T–T distances reveal small but significant variations, the $\overline{T-O}$ non brg. and the $\overline{T-O}$ are substantially constant. In Fig. 4 the most sensitive bond lengths are plotted against the electrons in the M2 site. The greatest values of $\overline{T-O}$ brg. occur in Di100, showing the straining effect of the M2 size on the chain. The ΔSi (= $\overline{T-O}$

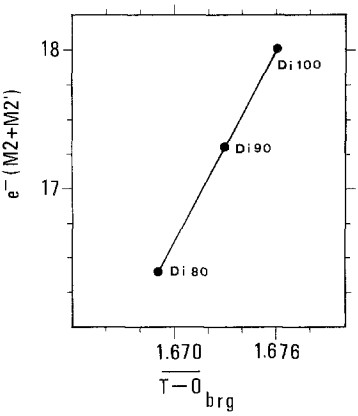

Fig. 4. $\overline{T-O}$ brg. bond lengths *vs.* e^- (M2 + M2') plot

brg. – $\overline{T-O}$ non brg.) (*Morimoto* et al., 1975) is in fact greatest in diopside and tends to decrease in Di90 and Di80. This shows how the release of the O3 atoms from M2′ causes the T–O3 lengths to become smaller (*Morimoto* et al., 1975) (Fig. 5).

The simplified projection normal to the *c*-axis (Fig. 6) shows the out-of-plane (100) tilting (*Cameron* et al., 1973; *Ohashi* and *Finger*, 1974) of the O2 oxygen atoms (out of plane angles listed in Table 5) occurring in the tetrahedral configuration by substitution of Ca by Mg in the M2 polyhedron. O2A and O2B apparently approach each other in the projection (from 2.597 Å in Di100 to 2.550 Å in Di80). This does not correspond to a real O2A–O2B distance which is maintained unchanged at 2.984 Å. Consequently only a slight collapse of the chain against its opposite one must have happened causing then a β angle variation.

The β angle is not only indicative of the movements among the chains but also of the single chain configuration. *Ribbe* and *Prunier* (1977) found a

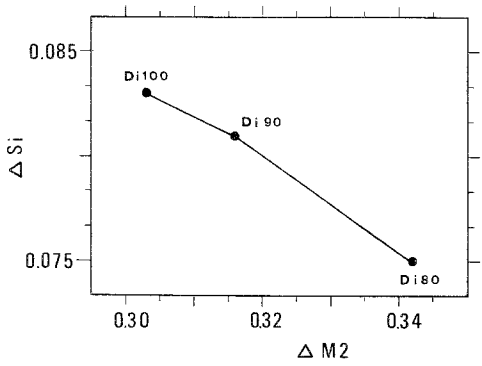

Fig. 5. Δ M2 *vs.* ΔSi plot. ΔSi (*Morimoto* et al., 1975) defined by $\overline{T-O}$ brg. – $\overline{T-O}$ non brg.

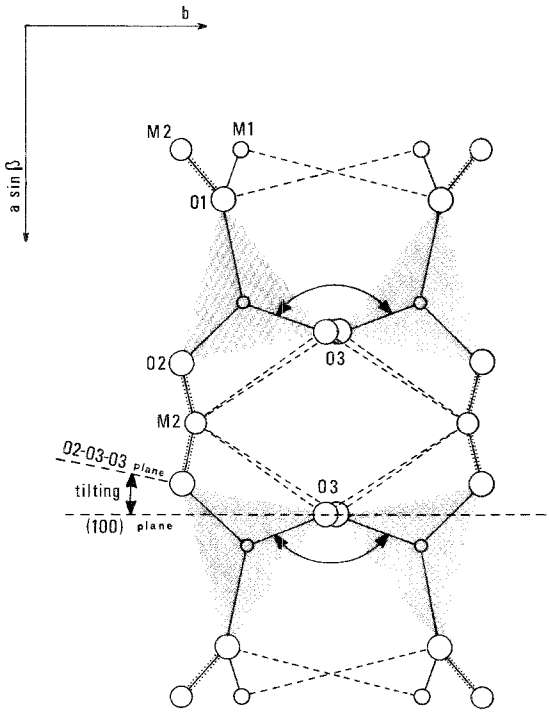

Fig. 6. Partial schematic projection of two opposite chains onto the plane normal to *c*-axis. Note how shortening bonds (▨) and lengthening bonds (– – – –) (with increase of En content) cause the out-of-plane (100) tilting with a relative variation of T–O3–T angle and the apparent approach of the O2 atoms

correlation between β and the chain rotation angle (O3A2–O3A1–O3A2). This is also found in our samples (Tables 1 and 5).
There is an even strong correlation between β and T–O3–T angle indicating both the tilting of the chain (Fig. 6) and the kinking.
Considering the Zn clinopyroxene framework, it is strange how with so high a kink (161.3°) in the chain the large c lattice parameter appears possible (5.296 Å) (compare with Di100, c = 5.251 Å, with rather modest kink = 166.1°). The study of the variation in the tetrahedral angle O3A1–T–O3A2 (111.2° in Zn clinopyroxene and 104.1° in Di100) explains how the inner transformation of the tetrahedron compensates the kinking of the chain. Variations similar to those in the diopside-Zn clinopyroxene chain occur in our samples also. However these are small in proportion to the limited number of M2′. Variation in the kinking angle from 166.1° (Di100) to 164.9° (Di80) corresponds to an increase of O3–T–O3 angle from 104.1° (Di100) to 104.9° (Di80). This way the c lattice parameter remains substantially constant.

Conclusions

As the data available from the X-Ray analysis depict only an average situation among a high number of cells, the double atomic position recognized for the M2 site and the structural variations in our samples must be treated as belonging to two different structural models. The first one belongs to diopside which is one of the end-members of our series and also the primary structural configuration in Di90 and Di80.
Furthermore we have seen the close similarity between the M2 site in the $ZnSiO_3$ (M) pyroxene (*Morimoto* et al., 1975) and M2′ characterizing Di90 and Di80 samples. Then the second structural model considered by us is that of $ZnSiO_3$ $C2/c$ pyroxene. The principal features of this pyroxene, in comparison with diopside, is the release from M2 cation of the O3 atoms and the strengthening of M2–O2 and M2–O1 bonds. As a consequence there is a considerable rearrangement in the chain as outlined below:
1) shortening of the $\overline{T-O}$ brg. distances by charge balance requirements from 1.676 Å in diopside to 1.626 Å in Zn clinopyroxene (1.669 Å in Di80);
2) kinking of the chain: O3A2–O3A1–O3A2 angle is 166.1° in diopside and 161.3° in Zn clinopyroxene (164.9° in Di 80);
3) tilting out of plane (100) varying from 2.3° in diopside to 6.0° in Zn clinopyroxene (3.1° in Di80).
Now it might be expected that the increase of En in the solid solution would cause continuous changes in the structural configuration of diopside towards that of $ZnSiO_3$ $C2/c$. The coexistence, in one phase, of M2′ and M2 sites, four- and eight-coordinated, could suggest an average structure affected by

Table 6. *Magnitudes and Orientations of the Principal Axes of the Thermal Vibration Ellipsoids* (estimated standard errors in parentheses)

	Ellipsoid axis, r_i	r.m.s. amplitude	angle (deg. of r_i with			r.m.s. amplitude	angle (deg.) of r_i with			r.m.s. amplitude	angle (deg.) of r_i with		
	i	(Å)	x	y	z	(Å)	x	y	z	(Å)	x	y	z
		M2				M1				T			
	1	0.066 (2)	111 (2)	90	143 (2)	0.060 (3)	122 (10)	90	132 (10)	0.058 (2)	165 (13)	85 (24)	88 (18)
Di100	2	0.084 (1)	90	0	90	0.072 (2)	90	0	90	0.060 (2)	94 (27)	34 (23)	56 (23)
	3	0.101 (1)	159 (2)	90	53 (2)	0.073 (3)	148 (10)	90	42 (10)	0.064 (2)	104 (12)	123 (21)	33 (21)
	1	0.057 (2)	110 (2)	90	143 (2)	0.057 (4)	102 (6)	90	152 (6)	0.056 (2)	168 (11)	102 (9)	78 (9)
Di90	2	0.094 (2)	90	0	90	0.072 (3)	90	0	90	0.062 (2)	101 (12)	48 (8)	41 (8)
	3	0.101 (2)	160 (2)	90	53 (2)	0.077 (3)	168 (6)	90	62 (6)	0.071 (2)	84 (5)	136 (7)	51 (7)
	1	0.057 (3)	114 (2)	90	139 (2)	0.064 (4)	90	180	90	0.056 (2)	108 (29)	157 (19)	97 (16)
Di80	2	0.103 (2)	24 (2)	90	131 (2)	0.069 (4)	53 (12)	90	53 (12)	0.060 (2)	22 (25)	104 (28)	122 (7)
	3	0.104 (2)	90	180	90	0.080 (3)	143 (11)	90	37 (11)	0.075 (2)	102 (5)	73 (5)	147 (5)
		O1				O2				O3			
	1	0.057 (5)	158 (10)	78 (6)	93 (11)	0.069 (4)	114 (5)	147 (7)	102 (9)	0.063 (4)	63 (13)	116 (4)	150 (6)
Di100	2	0.074 (4)	108 (11)	87 (15)	3 (12)	0.088 (3)	96 (14)	109 (10)	21 (12)	0.076 (4)	28 (13)	84 (8)	79 (12)
	3	0.085 (3)	102 (8)	168 (7)	88 (15)	0.098 (3)	155 (6)	65 (7)	73 (14)	0.101 (3)	97 (6)	153 (4)	63 (4)
	1	0.061 (4)	155 (10)	78 (10)	95 (11)	0.065 (4)	118 (4)	146 (3)	98 (5)	0.063 (4)	80 (15)	108 (4)	161 (5)
Di90	2	0.076 (3)	106 (23)	71 (64)	18 (62)	0.095 (3)	49 (7)	97 (6)	153 (7)	0.075 (4)	13 (12)	94 (7)	94 (14)
	3	0.079 (4)	107 (21)	157 (54)	72 (65)	0.112 (3)	125 (7)	57 (3)	111 (7)	0.101 (3)	98 (5)	161 (4)	71 (4)
	1	0.065 (5)	144 (17)	60 (18)	92 (11)	0.074 (5)	112 (6)	155 (4)	94 (5)	0.072 (4)	96 (45)	102 (9)	154 (37)
Di80	2	0.076 (5)	59 (19)	31 (18)	95 (28)	0.103 (4)	32 (6)	105 (6)	133 (6)	0.076 (4)	10 (29)	99 (11)	110 (43)
	3	0.083 (4)	74 (17)	96 (25)	174 (25)	0.127 (3)	112 (6)	70 (3)	136 (6)	0.110 (3)	98 (5)	164 (5)	75 (5)

positional disorder. As a matter of fact, the analysis of thermal ellipsoids of the oxygen atoms (Table 6) of Di90 and Di80 shows a rather limited anisotropy. This suggests that there is no significant positional disorder in the framework of our samples. Therefore the structure obtained by X-Ray diffraction can be considered close to the real structure characterized by a univocal framework configuration except for the M2 site in which Ca–Mg ordering can be appreciated. Such a framework positional order can be achieved because the tetrahedral chain absorbs the conspicuous variations occurred in the M2 polyhedron, with tilting and kinking. On the other hand, the limited M2′ occupancy found in Di80 (similar values in the M2′ occupancies have also been found in a lot of natural clinopyroxenes studied under the same experimental conditions (*Dal Negro* et al.,1982)) could suggest that, at least at low temperature, the amount of Mg occupying the M2′ site cannot be higher than in Di80 sample; this is consistent with the large miscibility gap between En and Di at low temperature.

It might be expected, from an examination of the crystals at high temperature, that the *C2/c* Ca-rich members would show a displacive transformation in the M2 site from an ordered M2–M2′ condition to a disordered one similar to that noted by *Ohashi* et al. (1975) in Hd–Fs series at room temperature. This disordered configuration at high temperature might account for a greater substitution of Ca by Mg in the M2 site and therefore an increased solid solution of En in Di.

Acknowledgements

We thank Prof. *A. Dal Negro* for the helpful suggestions and Prof. *S. Saxena* for revising the manuscript. "Centro di Studi per la Cristallografia Strutturale, Pavia" and "Centro di Studi sui biopolimeri, Padova" are gratefully acknowledged for diffractometer facilities. Thanks are due also to "Centro di Studio sui Problemi dell'Orogeno delle Alpi Occidentali, Torino" and to "Centro di Studio sui Problemi dell'Orogeno delle Alpi Orientali, Padova". This work was financed by C.N.R. (CT No. 80.02585.05).

References

Atlas, L., 1952: The polymorphism of $MgSiO_3$ and solid state equilibria in the system $MgSiO_3$–$CaMgSi_2O_6$. J. Geol. *60*, 125–147.

Biggar, G. M., O'Hara, M. J., 1969: A comparison of gel and glass starting materials for phase equilibrium studies. Min. Mag. *37*, 198–205.

Boyd, F. R., Schairer, J. F., 1964: The system $MgSiO_3$–$CaMgSi_2O_6$. J. Petrology *5*, 275–309.

Burnham, C. W., Clark, J. R., Papike, J. J., Prewitt, C. T., 1967: A proposed crystallographic nomenclature for clinopyroxene structure. Z. Krist. *125*, 109–119.

Busing, W. R., Martin, K. O., Levy, H. A., 1962: ORFLS, A Fortran Crystallographic Least-squares Program. Oak Ridge National Lab. Doc. ORNL-TM-305.

Cameron, M., Sueno, S., Prewitt, C. T., Papike, J. J., 1973: High-temperature crystal chemistry of acmite, diopside, hedenbergite, jadeite, spodumene, and ureyite. Amer. Min. *58*, 594–618.

– *Papike, J. J.,* 1981: Structural and chemical variations in pyroxenes. Amer. Min. *66*, 1–50.

Clark, J. R., Appleman, D. E., Papike, J. J., 1969: Crystal-chemical characterization of clinopyroxenes based on eight new structure refinements. Mineral. Soc. Amer. Spec. Pap. *2*, 31–50.

Dal Negro, A., Carbonin, S., Molin, M., Cundari, A., Piccirillo, E. M., 1982: Intracrystalline cation distribution in natural clinopyroxenes of tholeiitic, transitional and alkaline basaltic rocks. Advances in Physical Geochemistry 2. Berlin-Heidelberg-New York: Springer. (In press.)

Davis, B. T. C., Boyd, F. R., 1966: The join $Mg_2Si_2O_6$–$CaMgSi_2O_6$ at 30 kilobars pressure and its application to pyroxenes from kimberlites. J. Geophys. Res. *71*, 3567–3576.

Fleet, M. E., 1976: Distortion parameters for coordination polyhedra. Min. Mag. *40*, 531–533.

Hamilton, W. C., 1959: On the isotropic temperature factor equivalent to a given anisotropic temperature factor. Acta Cryst. *12*, 609–610.

Hornstra, J., Stubbe, B., 1972: PW1100 Data Processing Program. Eindhoven, Holland: Philips Research Laboratories.

International Tables for X-Ray Crystallography, Vol. IV (*Ibers, J. A., Hamilton, W. C.,* eds.), 1974: Birmingham: Kynoch Press.

Kushiro, I., 1972: Determination of liquidus relations in synthetic silicate systems with electron probe analysis: the system forsterite–diopside–silica at 1 atmosphere. Amer. Min. *57*, 1260–1271.

Levien, L., Prewitt, C. T., 1981: High-pressure structural study of diopside. Amer. Min. *66*, 315–323.

Lindsley, D. H., Dixon, S. A., 1976: Diopside–enstatite equilibria at 850° to 1400°C, 5 to 35 kb. Amer. J. Sci. *276*, 1285–1301.

Mori, T., Green, D. H., 1975: Pyroxenes in the system $Mg_2Si_2O_6$–$CaMgSi_2O_6$ at high pressure. Earth Planet. Sci. Letters *26*, 277–286.

Mori, T., Green, D. H., 1976: Subsolidus equilibria between pyroxenes in the CaO–MgO–SiO_2 system at high pressures and temperatures. Amer. Min. *61*, 616–625.

Morimoto, N., Appleman, D. E., Evans, H. T., 1960: The crystal structures of clinoenstatite and pigeonite. Z. Krist. *114*, 120–147.

– *Koto, K.,* 1969: The crystal structure of orthoenstatite. Z. Krist. *129*, 65–83.

– *Nakajima, Y., Syono, Y., Akimoto, S., Matsui, Y.,* 1975: Crystal structures of pyroxene-type $ZnSiO_3$ and $ZnMgSi_2O_6$. Acta Cryst. *B31*, 1041–1049.

Nehru, C. E., Wyllie, P. J., 1974: Electron microprobe measurement of pyroxenes coexisting with H_2O-undersaturated liquid in the join $CaMgSi_2O_6$–$Mg_2Si_2O_6$ at 30 kilobars, with applications to geothermometry. Contrib. Min. Petrol. *48*, 221–228.

Newton, R. C., Charlu, T. V., Anderson, P. A. M., Kleppa, O. J., 1979: Thermochemistry of synthetic clinopyroxenes on the join $CaMgSi_2O_6$–$Mg_2Si_2O_6$. Geochim. Cosmochim. Acta *43*, 55–60.

North, A. C. T., Phillips, D. C., Scott Mathews, F., 1968: A semi-empirical method of absorption correction. Acta Cryst. *A24*, 351–359.

Ohashi, Y., Finger, L. W., 1974: The effects of cation substitution on the symmetry and the tetrahedral chain configuration in pyroxenes. Carnegie Inst. of Washington Year Book *73*, 522–525.

– *Burnham, C. W., Finger, L. W.,* 1975: The effect of Ca–Fe substitution on the clinopyroxene crystal structure. Amer. Min. *60*, 424–434.

– *Finger, L. W.,* 1976: The effect of Ca substitution on the structure of clinoenstatite. Carnegie Inst. of Washington Year Book *75*, 743–746.

Ribbe, P. H., Prunier, A. R., Jr., 1977: Stereochemical systematics of ordered *C2/c* silicate pyroxenes. Amer. Min. *62*, 710–720.

Robinson, K., Gibbs, G. V., Ribbe, P. H., 1971: Quadratic elongation; a quantitative measure of distortion in coordination polyhedra. Science *172*, 567–570.

Rossi, G., Tazzoli, V., Ungaretti, L., 1978: Crystal-chemical studies on sodic clinopyroxenes. Proceed. 11th IMA Meeting, Novosibirsk.

Schwab, R. G., Schwerin, M., 1975: Polymorphie und Entmischungsreaktionen der Pyroxene im System Enstatit ($MgSiO_3$)-Diopsid($CaMgSi_2O_6$). N. Jb. Miner. Abh. *124*, 223–245.

Shannon, R. D., Prewitt, C. T., 1969: Effective Ionic Radii in Oxides and Fluorides. Acta Cryst. *B25*, 925–946.

Smith, J. V., 1959: The crystal structure of proto-enstatite, $MgSiO_3$. Acta Cryst. *12*, 515–519.

– 1969: Crystal structure and stability of the $MgSiO_3$ polymorphs: Physical properties and phase relations of Mg, Fe pyroxenes. Mineral. Soc. Amer. Spec. Pap. *2*, 3–29.

Takeda, H., 1972: Crystallographic studies of coexisting aluminan orthopyroxene and augite of high-pressure origin. J. Geophys. Research *77*, 5798–5811.

Tokonami, M., 1965: Atomic scattering factor for O^{2-}. Acta Cryst. *19*, 486.

Warner, R. D., Luth, W. C., 1974: The diopside-orthoenstatite two-phase region in the system $CaMgSi_2O_6$–$Mg_2Si_2O_6$. Amer. Min. *59*, 98–109.

Zachariasen, W. H., 1963: The secondary extinction correction. Acta Cryst. *16*, 1139–1144.

Authors' addresses: Prof. *E. Bruno*, Istituto di Mineralogia, Cristallografia e Geochimica, Università di Torino, Via S. Massimo 22, I-10123 Torino, Italy; Dr. *Susanna Carbonin* and Dr. *G. Molin*, Istituto di Mineralogia e Petrologia, Università di Padova, Corso Garibaldi 37, I-35100 Padova, Italy.